Clinical Epigenetics

RESEARCH

Open Access

PER3 promoter hypermethylation correlates to the progression of pan-cancer

Yaoxu Li[1,2†], Wenjuan Li[3†], Jinhai Deng[2] and Mingzhu Yin[2,4,5*]

Abstract

Background Malignant cells exhibit reduced period circadian regulator 3 (PER3) expression. However, the underlying mechanisms of variations in PER3 expression in cancers and the specific function of PER3 in tumor progression remain poorly understood.

Results We explored multiple public databases, conducted bioinformatics analyses, and performed in vitro and in vivo experiments for validation. We found PER3 expression was decreased in most types of cancers, and PER3 downregulation was associated with a poor prognosis in 8 types of cancer. PER3 promoter methylation levels were increased in 11 types of cancer. Promoter hypermethylation (CpG islands [CGIs] cg12258811 and cg14204433) correlated with decreased PER3 expression in six cancers (breast invasive carcinoma, colon adenocarcinoma, head and neck squamous cell carcinoma, kidney renal papillary cell carcinoma [KIRP], lung adenocarcinoma [LUAD], and uterine corpus endometrial carcinoma). CGI cg12258811 hypermethylation was associated with reduced survival time and advanced cancer stages. Moreover, the bisulfite pyrosequencing assay confirmed CGI cg12258811 hypermethylation and its negative correlation with PER3 expression. In vitro and in vivo experiments demonstrated that PER3 inhibited KIRP and LUAD progression. Decitabine enhanced PER3 expression and inhibited KIRP cell functions by reducing promoter (cg12258811) methylation level.

Conclusions Our findings advanced the mechanistic understanding of variations in PER3 expression in cancers and confirmed the tumor-associated function of PER3 hypermethylation and downregulation.

Keywords Period circadian regulator 3, Promoter, Methylation, Pan-cancer, Kidney renal papillary cell carcinoma, Lung adenocarcinoma

†Yaoxu Li, and Wenjuan Li have contributed equally.

*Correspondence:
Mingzhu Yin
yinmingzhu2008@126.com
[1] Department of Stomatology, Chongqing University Three Gorges Hospital, School of Medicine, Chongqing University, Wanzhou District, Chongqing 404100, China
[2] Clinical Research Center (CRC), Medical Pathology Center (MPC), Cancer Early Detection and Treatment Center (CEDTC) and Translational Medicine Research Center (TMRC), Chongqing University Three Gorges Hospital, School of Medicine, Chongqing University, Wanzhou District, Chongqing 404100, China
[3] Department of Emergency and Critical Care Medicine, The First Afliated Hospital of Chongqing Medical University, Chongqing 400016, People's Republic of China
[4] Chongqing Technical Innovation Center for Quality Evaluation and Identification of Authentic Medicinal Herbs, Wanzhou District, Chongqing 404100, China
[5] Three Gorges Hospital & Academy for Advanced Interdisciplinary Technology, CQU-Ferenc Krausz Nobel Laureate Scientific Workstation, Chongqing University, Chongqing, China

Introduction

Cancer is the leading cause of morbidity and mortality, limiting global life expectancy. In 2022, International Agency for Research on Cancer reported approximately 20 million new cancer cases and an estimated 9.7 million cancer-related deaths worldwide [1]. Despite significant advances in clinical cancer treatment strategies such as surgery, radiochemotherapy, and targeted therapy, the prognosis and survival rate for patients with cancer remain inadequate [2]. Therefore, discovering novel, effective biomarkers for diagnosis and potential therapeutic targets for treatment is critical [3].

Circadian clock genes are closely related to tumorigenesis and tumor advance [4]. Period circadian regulator 3 (PER3) is a member of Period genes involved in the circadian clock autoregulatory negative feedback transcriptional network. PER3 is upregulated by transcriptional activators CLOCK/BMAL1 heterodimers at the beginning of the cycle. Then, it binds with other Period (PER1/2) and Cryptochrome (CRY1/2) proteins via the PER-ARNT-SIM domains to form dimers, which interact with CLOCK and BMAL1 and repress the expressions of their own and other core clock genes and clock-controlled genes [5, 6].

Generally, expression levels of PER3 are altered in a range of cancers, and PER3 downregulation is associated with oncogenesis, tumor progress, and worse prognosis in some cancers, such as colon and rectal cancer, breast cancer, head and neck squamous carcinoma (HNSC), and kidney renal clear cell carcinoma (KIRC) [7–12]. More specifically, PER3 correlates with immune infiltrations, suppresses stemness, chemotherapy resistance, proliferation, and metastasis, and promotes autophagy and apoptosis of cancer cells [11, 13–16]. The downstream mechanisms involve regulating WNT/β-catenin, Notch, and MEK/ERK signaling pathways [9, 14, 17]. Moreover, PER3 gene mutations like variable number of tandem repeats and single nucleotide polymorphism increase the incidence of cancers [18–20].

However, the causes of altered PER3 expression in cancers and the specific molecular mechanism in PER3 regulating tumor progress remain poorly understood.

Epigenetic alterations are common during the onset and progression of cancer [21]. DNA methylation is a common epigenetic alteration that regulates gene expression by altering chromatin structure, DNA conformation, DNA stability, and the interaction between DNA and protein without modifying the nucleotide sequence [22, 23]. Hypermethylation of CpG islands (CGIs) in the gene promoter region results in gene silencing, whereas DNA hypomethylation in the same region causes gene reactivation [22]. Because DNA methylation is dynamic and reversible, it is a potential therapeutic target for cancer [24]. Consequently, the methylation of the promoter region of tumor suppressor genes has been extensively explored in recent years [25]. The tumor-suppressive action of PER3 has been confirmed in many cancers, however, its epigenetic alterations in cancers have received less attention [18]. In non-small cell lung cancer, reduced PER3 expression is associated with promoter region hypermethylation [26]. Whether PER3 expression is regulated by methylation alterations in the promoter region and the effect of such alterations on cancer prognosis in pan-cancer remains unclear and requires further investigations.

This study aimed to investigate the expression patterns, distinct prognostic values, and potential functions of PER3, as well as the methylation of its promoter region in pan-cancer. Specifically, we analyzed the differential expression and promoter methylation status of PER3 and their associated clinical parameters, prognostic prediction functions, immune infiltrations, and molecular mechanisms in pan-cancer cases using multilevel data from 33 cancers in the Cancer Genome Atlas (TCGA) and other large public databases. Furthermore, in vitro and in vivo validation experiments were conducted on kidney renal papillary cell carcinoma (KIRP) and lung adenocarcinoma (LUAD).

Materials and methods

mRNA expression of PER3 and prognostic analysis

The dysregulation of PER3, CLOCK, and BMAL1 expression across various types of cancer and normal tissues was investigated by combining the RNASeqV2 data of 33 cancers from TCGA (https://tcga.xenahubs.net) and data for 31 different normal tissues from the genotype-tissue expression (GTEx) database (http://commonfund.nih.gov/GTEx/) [27]. Prognosis analyses related to PER3 expression, including overall survival (OS), disease-specific survival (DSS), and progression-free interval (PFI), were performed in various cancers using Kaplan–Meier (K–M) curves based on COX regression analysis. Additionally, the correlations between mRNA expression of PER3 and tumor (T), node (N), and metastasis (M) stages were analyzed. The gene expression data were further standardized by log2 conversion, and the "survminer" and "ggplot2" R packages were used for survival analysis and visualizations, respectively.

UALCAN analysis

The UALCAN portal (http://ualcan.path.uab.edu/index.html) was used to investigate PER3 promoter methylation levels in different cancers and their corresponding normal tissues. Additionally, the associations between individual cancer stages and PER3 promoter methylation

levels and mRNA expressions were analyzed using the UALCAN portal [28].

Region-specific methylation analysis of the PER3 promoter

The MEXPRESS database (https://mexpress.be/) was used to study the relationship between the methylation levels of specific promoter probe-associated CGIs and PER3 mRNA expression [29]. RNAseq and Illumina human methylation 450 data downloaded from TCGA were analyzed and visualized using the "ggplot2" R package to validate the MEXPRESS database results. Moreover, the Epigenome-Wide Association Study (EWAS) Data Hub database (https://ngdc.cncb.ac.cn/ewas/datahub/index) was used to investigate differences in promoter CGI methylation levels between multiple cancers and normal tissues [30].

Prognostic analysis of the methylation level of promoters and specific CGIs

The relationship between OS of patients with breast invasive carcinoma (BRCA), colon adenocarcinoma (COAD), head and neck squamous cell carcinoma (HNSC), KIRP, LUAD, and uterine corpus endometrial carcinoma (UCEC) and methylation levels of promoter and CGI were analyzed using the EWAS Data Hub database. Additionally, the MethSurv database (https://biit.cs.ut.ee/methsurv/) was used as a backup when data was unavailable in the EWAS Data Hub database [31].

Immune cell infiltration analysis

The original level 3 HTSeq-FPKM RNAseq data for BRCA, COAD, HNSC, KIRP, LUAD, and UCEC were downloaded from TCGA. Subsequently, the "gene set variation analysis" R package was used to perform the infiltration analysis of 24 immune cell markers [32, 33].

Gene enrichment analysis

The top 200 differentially expressed genes (DEGs) associated with PER3 expression in BRCA, COAD, HNSC, KIRP, LUAD, and UCEC from TCGA were obtained using the "DESeq2" R package. The Kyoto Encyclopedia of Genes and Genomes (KEGG) pathway analysis and Gene Ontology (GO) enrichment analysis of the top 200 DEGs associated with PER3 were performed by the "clusterProfiler" R package.

Cell cultures and reagents

Human Kidney-2 (HK-2) cells, KIRP cell lines 786-O and Caki-2, and LUAD cell line A549 were obtained from Wuhan Pricella Biotechnology Co., Ltd. (Wuhan, China). All cell lines were identified by short tandem repeat sequence analysis and confirmed to be mycoplasma contamination-free. HK-2 and A549 cells were cultured with Dulbecco's Modified Eagle Medium (Gibco, USA). 786-O and Caki-1 cells were incubated in Roswell Park Memorial Institute-1640 (Pricella, China) and McCoy's 5A (Pricella, China), respectively. Subsequently, all the cells were incubated in a medium mixture comprising 89% medium, 10% fetal bovine serum (FBS) (PAN-biotech, Germany), and 1% penicillin–streptomycin (Pricella, China) at 37 °C with 5% CO_2.

Quantitative real-time polymerase chain reaction (RT-qPCR)

Total RNA was extracted using an RNA Isolation Total RNA Extraction Reagent (R401-01, Vazyme, China) following the instruction manual. RNA purity and concentration were evaluated using microscopic spectrophotometry (Nanodrop, Thermo Fisher Scientific, USA), followed by reverse transcription into cDNA using the RT Master Mix for qPCR II (gDNA digester plus) kit (HY-K0511A, MedChemExpress, USA). RT-qPCR was performed on the CFX Connect Real-Time System (1,855,201, BIO-RAD, USA) using the SYBR Green qPCR Master Mix (No ROX) (HY-K0523, MedChemExpress, USA). Primers for PCR analysis were designed using Oligo (version 7.0) software. The sequences are presented in Supplemental Table S1.

Western blotting

The cell protein was extracted using a 100:1 mixture of RIPA lysis solution (P0013B, Beyotime, China) and phenylmethanesulfonyl fluoride (ST506, Beyotime, China). The wet transfer method was used to transfer protein to polyvinylidene fluoride (PVDF) membranes (IPVH00010, Millipore, USA). The PVDF membranes were soaked in 5% skimmed milk at 25 °C for 2 h, incubated in the primary antibody working solutions at 4 °C overnight, and incubated in secondary antibodies at RT for 1 h. The proteins on the PVDF membranes were visualized using a chemiluminescence imaging system (FUSION FX, VILBER, France). Details of the antibodies are displayed in Supplemental Table S2. GAPDH was used as a loading control. Protein band gray values were analyzed using Image J (version 5.0) software.

Construction of stable PER3-overexpressed and PER3-silenced cell lines

The PER3 overexpressed and silenced vectors and their corresponding control vectors were designed and synthesized by Hanbio (Shanghai, China). Primers for PER3 amplification and deletion were constructed based on the PER3 mRNA sequence (GenBank Accession: NM_016831). The primer sequences are provided in Supplemental Table S3. 786-O, Caki-1, and A549 cells were infected with PER3-overexpressed (PER3) or PER3-free

(Vector) lentivirus. HK-2 cells were infected with PER3-silenced (sh-PER3#1 and sh-PER3#2) or the control (sh-NC) lentivirus.

The cells were screened with 2 μg/mL puromycin to obtain stable PER3-overexpressed and PER3-silenced cells and their corresponding negative controls.

Colony formation assay

786-O, Caki-1, HK-2, and A549 cells were seeded into 6-well plates. The 786-O, HK-2, and A549 cells were cultured for 10 days (1000 cells per well), and the Caki-1 cells were cultured for 14 days (2000 cells per well). Subsequently, the cells were fixed and stained with crystal violet for 30 min. Images were captured using a chemiluminescence imaging system.

CCK-8 assay

The cell counting Kit-8 (HY-K0301, MedChemExpress, USA) was used to evaluate cell proliferation. A 100 μL cell suspension (1×10^4 cells/mL) was added to the 96-well plate and incubated overnight at 37 °C with 5% CO_2. Subsequently, 100 μL of medium (10% CCK-8 reagent) was added to each well at 24, 48, 72, and 96 h. The plate was incubated for 2 h before being measured for optical density at 450 nm using an enzyme labeling instrument (BioTek, USA).

Wound healing assay

The cells were seeded in a serum-free medium and starved for 24 h. Subsequently, the cell monolayers were scratched with a sterile 200-mL pipette tip and starved for another 24 h. Images of the scratches were captured using a microscope (IX73, Olympus, Japan) (×40 and ×100) at 0 and 24 h.

Transwell migration and invasion assays

Transwell assays were conducted using Transwell chambers (3422, Corning, USA) precoated with Matrigel (356,234, Corning, USA) for invasion or without Matrigel for migration. The lower chambers were plated with 10% FBS (600 μL), whereas the upper chambers were filled with FBS-free medium containing 1×10^5 cells (200 μL). After culturing for 24 h, cells on the surface of the Transwell chambers were fixed with methyl alcohol, stained with crystal violet, and counted using a microscope at ×40 and ×200 magnifications.

In vivo xenograft tumor models

All procedures were approved by the Institutional Animal Care and Use Committee of Chongqing Medical University (approval number: IACUC-CQMU-2024-0462). Male BALB/c nude mice (age: 5–6 weeks old, weight: 18–21 g) were sourced from Changzhou Cavens Laboratory Animal Co., Ltd. (China) and housed under specific-pathogen-free conditions. The mice were randomly divided into two groups (n = 5 per group) and injected subcutaneously with vector-786-O (control group) or PER3-786-O cells (experimental group). After feeding for 25 days, the mice were euthanized by cervical dislocation, and tumors were excised. Tumors were measured for their maximum diameter (a), minimum diameter (b), and weight. Tumor volume was calculated as $0.5\times a\times b^2$. The harvested tumors were used for immunohistochemistry (IHC) and hematoxylin–eosin (H&E) staining.

IHC staining

IHC staining was conducted using a DA1010 IHC detection kit (Solarbio, Beijing, China). Routinely treated paraffin sections were incubated with the PER3 primary antibody overnight at 4 °C and incubated with the secondary antibody at RT for 2 h. Details of the antibodies are provided in Supplemental Table S2. The sections were dehydrated and sealed following diaminobenzidine development and hematoxylin redyeing. Images were captured using microscopy, and results were analyzed using semiquantitative and double-grading methods [34].

Decitabine (DAC) treatment and bisulfite pyrosequencing (BSP) analysis

Cells (1.5×10^5) were seeded on 6 cm dishes, incubated overnight at 37 °C, and treated with 10 μM DAC (HY-A0004, MCE, USA) for 72 h, with the medium and drug replaced every 24 h. DMSO was used in the control group. The MethPrimer website (https://urogene.org/cgi-bin/methprimer/methprimer.cgi) was used to predict the PER3 promoter CGIs [35]. BSP was performed with the assistance of Sangon Biotech (Shanghai, China) using HK-2, 786-O, and Caki-1 cells. Primer sequences for BSP are displayed in Supplemental Table S4.

Statistical analysis

R language software [R-3.6.3, 64-bit] was used for all R-related analyses. Results from more than three independent repetitions are presented as mean ± standard deviation (SD). The Student's t-test was used to compare two groups of independent samples. In all analyses, $P<0.05$ was considered statistically significant (ns indicated not significant ($P\geq0.05$), * indicated $P<0.05$, ** indicated $P<0.01$, *** indicated $P<0.001$, and **** indicated $P<0.0001$, respectively).

Results

Pan-cancer expression landscape of PER3

The transcription levels of PER3 were analyzed using the TCGA and GTEx databases (Fig. 1A). Generally, PER3

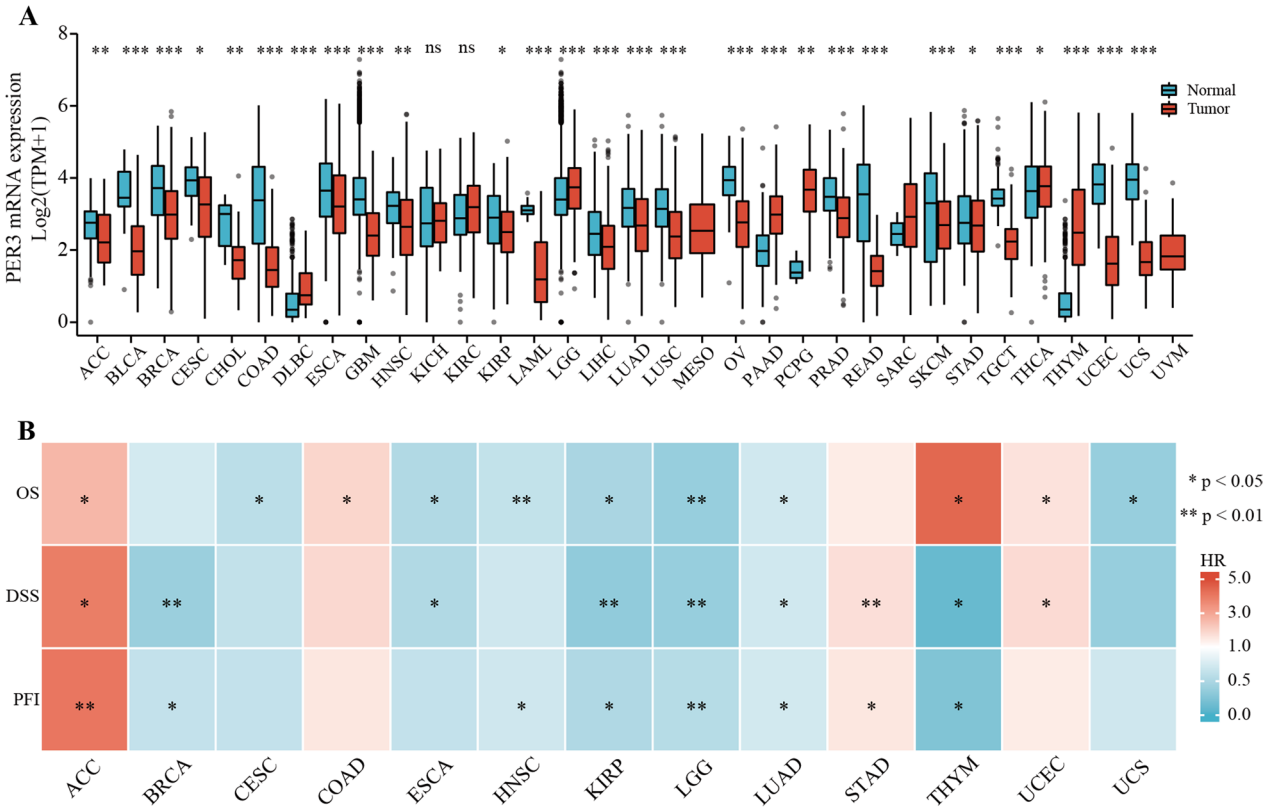

Fig. 1 **A** Dysregulated PER3 mRNA expression in pan-cancer. **B** Correlations between PER3 expression and OS, DSS, and PFI in pan-cancer (with significant differences in OS or DSS and PFI). ns, not significant; **P* < 0.05; ***P* < 0.01; and ****P* < 0.001

mRNA expression was significantly lower in tumors than that in normal tissues across most cancers (n = 22) (*P* < 0.05). Specifically, in lymphoid neoplasm diffuse large B-cell lymphoma, brain lower grade glioma (LGG), pancreatic adenocarcinoma, pheochromocytoma and paraganglioma, thyroid carcinoma, and thymoma (THYM), PER3 expression was significantly higher in tumors than that in normal samples (*P* < 0.05). However, no significant difference in PER3 expression was observed between the tumor group and the normal tissue group in kidney chromophobe and KIRC (*P* > 0.05). Data on PER3 expression in normal tissues corresponding to mesothelioma and uveal melanoma were unavailable in the databases, and the number of relevant normal tissues for sarcoma was insufficient for analysis (n = 2).

Pan-cancer analysis of the multifaceted prognostic value of PER3

Based on the 28 cancers exhibiting significant differential PER3 expression between tumors and corresponding normal tissues, the survival curves of OS, DSS, and PFI were used to confirm the effects of PER3 expression levels on patient prognosis. Cancers exhibiting significant differences in OS or DSS and PFI were considered for further studies (Fig. 1B). The results demonstrated that higher PER3 expression can improve patient prognosis in eight cancer types (hazard ratio [HR] < 1; *P* < 0.05): BRCA, cervical squamous cell carcinoma and endocervical adenocarcinoma (CESC), esophageal carcinoma (ESCA), HNSC, KIRP, LGG, LUAD, and uterine carcinosarcoma (UCS). Conversely, high PER3 expression was associated with unfavorable OS or DSS and PFI in adrenocortical carcinoma (ACC), COAD, stomach adenocarcinoma (STAD), THYM, and UCEC (HR < 1; *P* < 0.05). Notably, the OS result for THYM differed from that of DSS and PFI. Detailed K–M curves for OS, DSS, and PFI are presented in Supplemental Fig. S1.

Pan-cancer promoter methylation landscape of PER3

Because promoter methylation regulates gene expression in cancer, we investigated PER3 promoter methylation levels in pan-cancer. Results revealed significantly higher PER3 promoter methylation levels in 11 cancers (*P* < 0.05) (BRCA, CHOL, COAD, GBM, HNSC, KIRP, LUAD, LUSC, PRAD, READ, and UCEC) compared with their corresponding normal tissues (Fig. 2). Considering the effects of PER3 on prognosis of patients with ACC, BRCA, CESC, COAD, ESCA, HNSC, KIRP, LGG, LUAD,

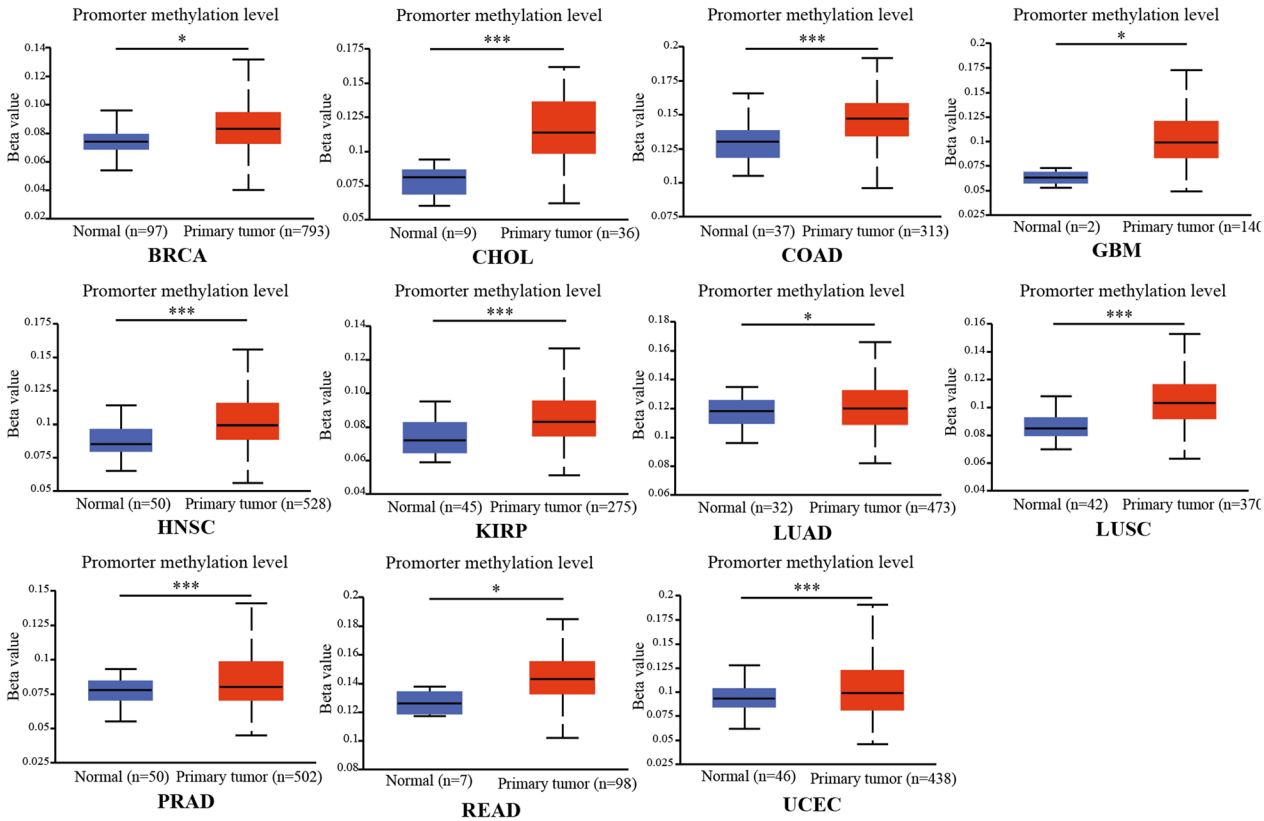

Fig. 2 Hypermethylation of PER3 promoter in pan-cancer. Data are presented as mean ± SD. **P* < 0.05; ***P* < 0.01; and ****P* < 0.001

STAD, THYM, UCEC, and UCS, subsequent analyses focused on six cancers (BRCA, COAD, HNSC, KIRP, LUAD, and UCEC). We also investigated the expression levels of PER3's transcription factors CLOCK and BMAL1 in pan-cancer (Supplemental Fig. S2A–B). Downregulation of CLOCK or BMAL1 occurred in bladder urothelial carcinoma (BLCA), BRCA, COAD, KICH, KIRC, KIRP, LUAD, PCPG, PRAD, THCA, and UCEC. The simultaneous CLOCK and BMAL1 expression increase occurred only in LIHC and STAD ($P < 0.05$).

Promoter CGI methylation correlates with the downregulation of PER3 mRNA expression

To further investigate PER3 promoter methylation levels in the aforementioned six cancers, the promoter CGI methylation levels and their relationships with PER3 mRNA expression were studied (Fig. 3). Results revealed a negative association between PER3 expression and the methylation levels of CGIs cg12258811 and cg14204433 in BRCA, COAD, HNSC, KIRP, LUAD, and UCEC ($P < 0.05$). Furthermore, the hypermethylation of CGI cg11753033 correlated with reduced PER3 expression in HNSC, KIRP, and UCEC ($P < 0.05$). Additionally, CGI cg11843502 methylation inhibited PER3 expression in LUAD and UCEC ($P < 0.05$). In UCEC, higher methylation levels of CGI cg06487986 or cg23927002 were associated with reduced PER3 expression ($P < 0.05$). The methylation profiles of these promoter regions in BRCA, COAD, HNSC, KIRP, LUAD, and UCEC, as well as their corresponding normal tissues, are displayed in Supplemental Fig. S3.

Prognostic value of methylation in the PER3 promoter

We evaluated the relationship between patient OS and the methylation level of promoter and PER3 expression-related promoter CGIs in the six cancers. Figure 4 depicts the results for all promoters and OS-related promoter CGIs. Additionally, Supplemental Fig. S4 presents the results of promoter CGIs that were non-significantly correlated with OS ($P > 0.05$). Except for Fig. 4G and S4C and F (from MethSurv), all analyses were performed using the EWAS Data Hub database. Higher promoter methylation was associated with poor OS in BRCA and LUAD ($P < 0.05$) (Fig. 4A and E). Moreover, high methylation levels of CGIs cg12258811 in KIRP and cg11843502 in LUAD reduced OS ($P < 0.05$) (Fig. 4G–H). However, increased methylation levels of the CGI cg14204433

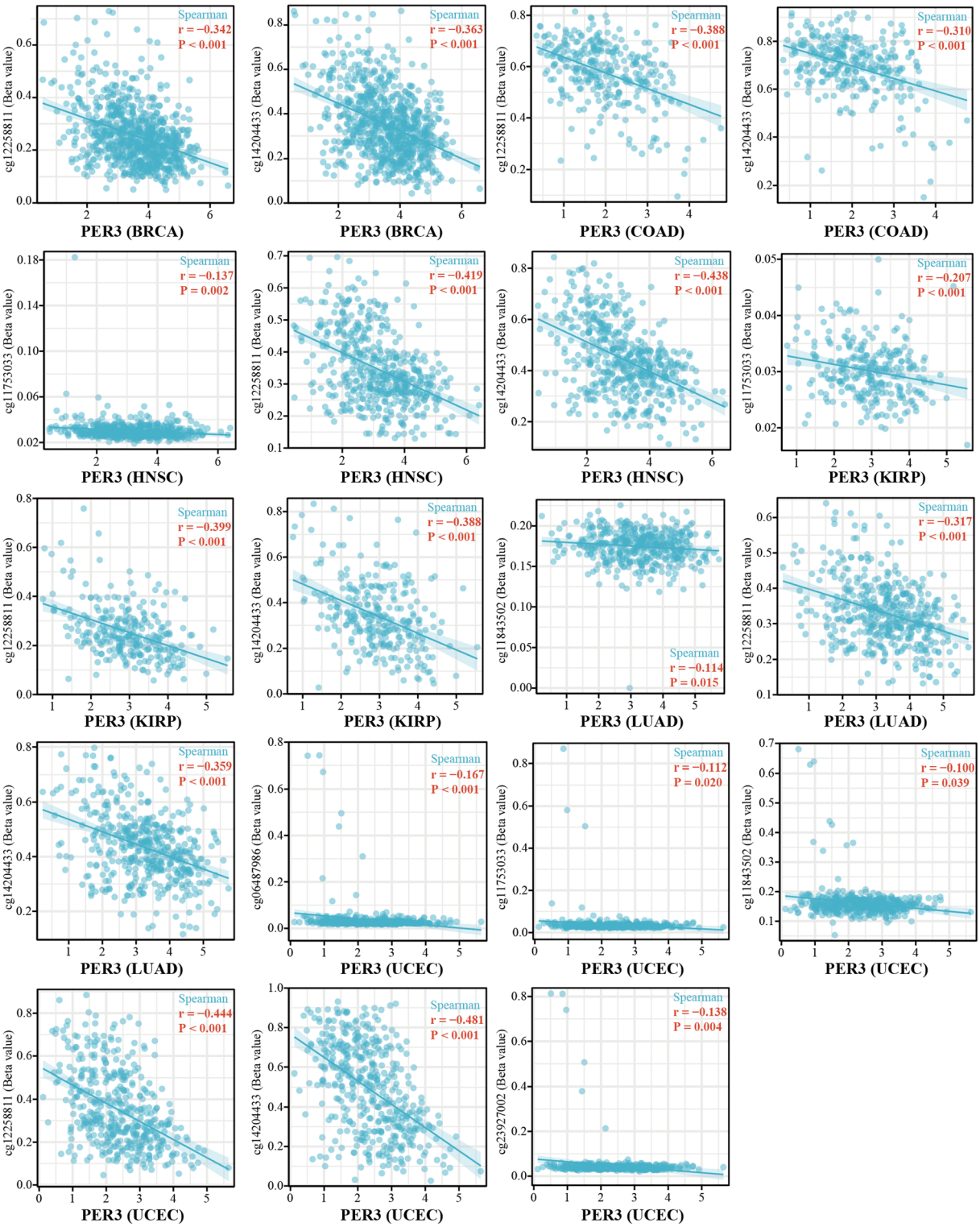

Fig. 3 Relationship between the methylation levels of PER3 promoter CGIs and mRNA expression in six cancers (BRCA, COAD, HNSC, KIRP, LUAD, and UCEC)

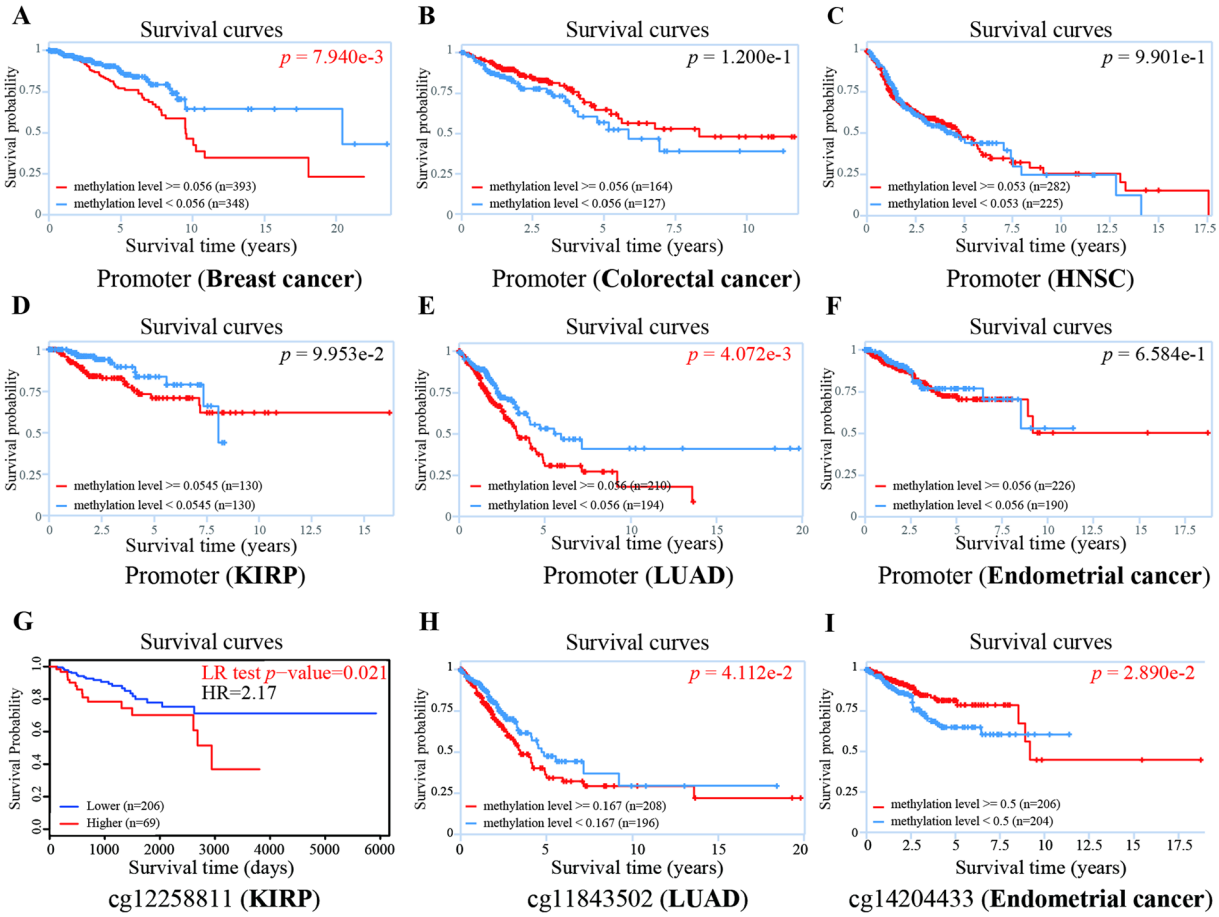

Fig. 4 Relationship between OS and methylation levels of PER3 promoter and specific CGIs in six cancers. The promoter of **A** breast cancer; **B** colorectal cancer; **C** HNSC; **D** KIRP; **E** LUAD; and **F** endometrial cancer. **G**–**I** Promoter CGI **G** cg12258811 in KIRP, **H** cg11843502 in LUAD, and **I** cg14204433 in endometrial cancer

in UCEC were associated with improved OS ($P<0.05$) (Fig. 4I).

PER3 promoter methylation level and mRNA expression vary in different cancer stages

Figure 5D depicts that stages 3 and 4 of KIRP exhibited significantly higher PER3 promoter methylation levels than stage 1 ($P<0.05$). Conversely, LUAD and UCEC exhibited decreased PER3 promoter methylation levels in the advanced stage ($P<0.05$) (Fig. 5E–F). Furthermore, stage 3 PER3 expression was significantly lower than that of stage 1 in BRCA and LUAD ($P<0.05$) (Fig. 5G and K). However, stage 3 PER3 expression was significantly higher than that of stage 1 in UCEC ($P<0.05$) (Fig. 5L). In KIRP, stage 4 PER3 expression was significantly reduced compared with those of stages 1 and 3 ($P<0.05$) (Fig. 5J). In COAD, stage 3 PER3 expression was significantly higher than that of stages 2 and 4 ($P<0.05$) (Fig. 5H). However, PER3 promoter methylation levels of patients with BRCA, COAD, and HNSC and PER3 expression in HNSC were uncorrelated to individual cancer stages ($P>0.05$) (Figs. 5A–C and I). Moreover, the correlation between the cancer stages and PER3 expression was analyzed in six cancers, excluding UCEC, due to the lack of corresponding data in TCGA (Supplemental Fig. S2C). The reduced PER3 was associated with advanced T stages in BRCA, HNSC, and LUAD ($P<0.05$). In KIRP and LUAD, PER3 downregulation correlated with worse N stages ($P<0.05$). However, PER3 expression was uncorrelated with the T, N, or M stage of COAD ($P>0.05$).

PER3 expression and immune cell infiltration

The results of PER3 expression-related infiltration analysis of immune cells are displayed in Fig. 6 and S5. In all six cancers, we discovered a significant positive correlation between PER3 expression and central memory T cell (TCM) and T helper cell infiltration ($P<0.05$). Moreover, higher eosinophil and mast cell infiltrations were associated with increased PER3 expression in all six cancers except UCEC ($P<0.05$). Furthermore,

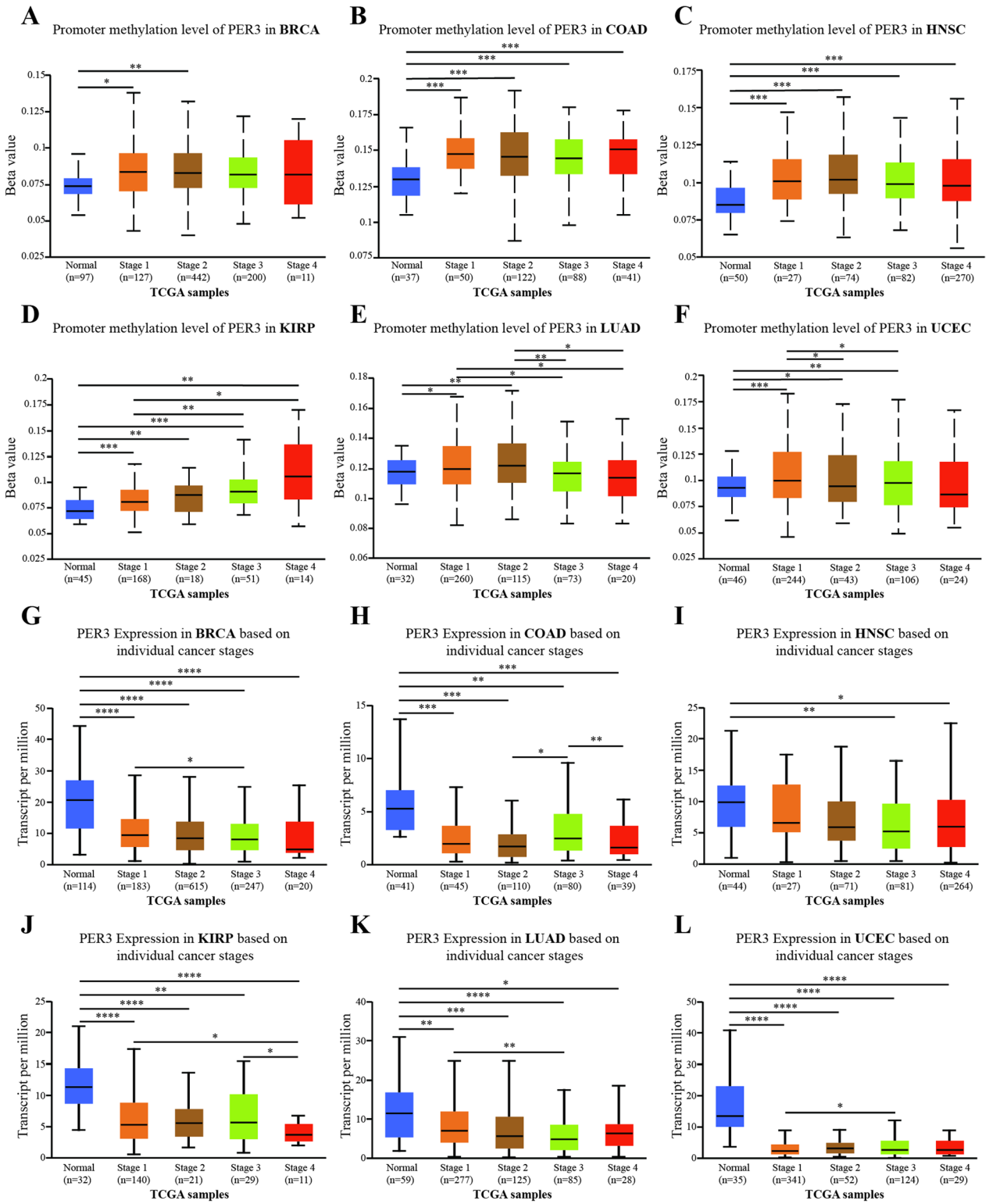

Fig. 5 **A**–**F** PER3 promoter methylation level and **G**–**L** PER3 expression in different individual cancer stages in six cancers. Data are presented as mean ± SD. *$P < 0.05$; **$P < 0.01$; ***$P < 0.001$; and ****$P < 0.0001$

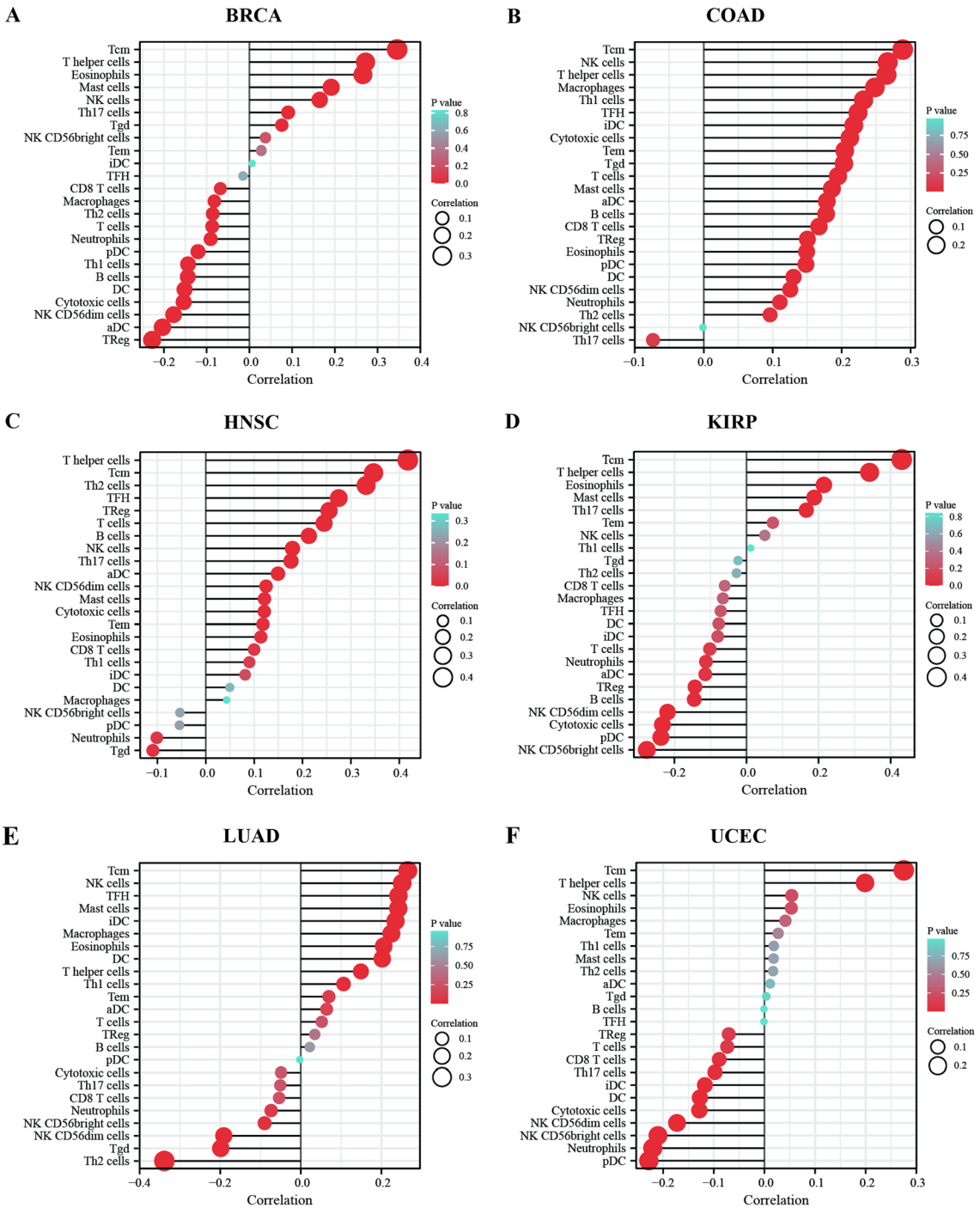

Fig. 6 PER3 expression correlates with immune infiltration in six cancers. **A** BRCA; **B** COAD; **C** HNSC; **D** KIRP; **E** LUAD; **F** UCEC

elevated PER3 expression was strongly associated with natural killer (NK) cell infiltration in BRCA, COAD, HNSC, and LUAD ($P < 0.05$). Specifically, high PER3 expression was associated with increased infiltration of most immune cells in COAD and HNSC (Fig. 6B–C). In BRCA and KIRP, PER3 levels were negatively correlated with regulatory T (Treg) cell infiltration (Fig. 6A and D).

Enrichment analysis of PER3 expression-related DEGs

We further investigated the molecular mechanism in which PER3 was involved (Fig. 7). "humoral immune

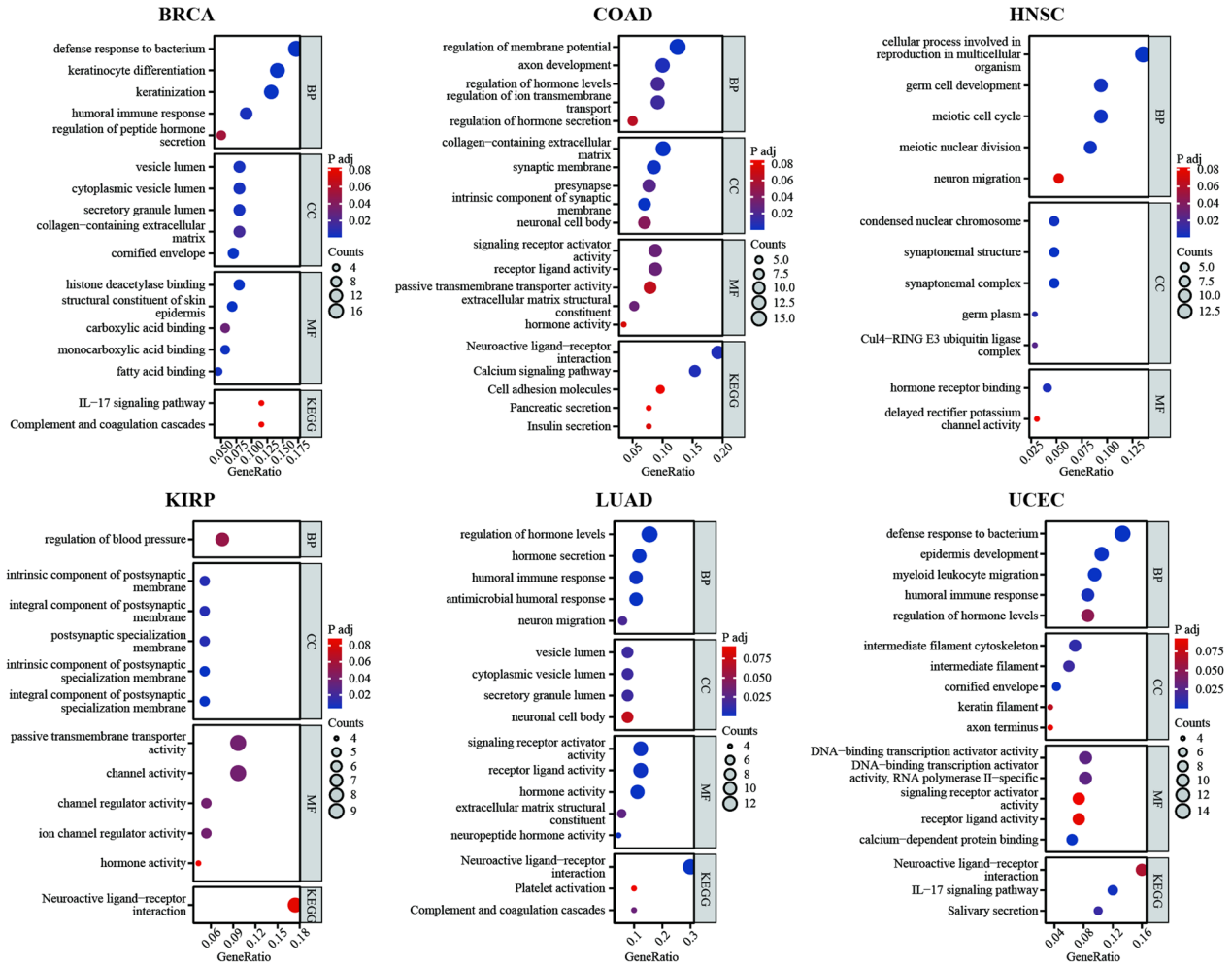

Fig. 7 Distributions of PER3-associated GO and KEGG pathways in six cancers

response" and "defense response to bacterium" were enriched in biological processes (BP) of BRCA, LUAD, and UCEC. Hormone-related BP "regulation of hormone levels" and "regulation of hormone secretion" were abundant in BRCA, COAD, LUAD, and UCEC. "neuron migration" occurred in BP of HNSC and LUAD. Neurological function-related cellular components (CC), like "synaptic membrane", "synaptonemal structure", "intrinsic component of postsynaptic membrane", and "neuron cell body" were broadly enriched in COAD, HNSC, KIRP, and LUAD. "vesicle lumen", "cytoplasmic vesicle lumen", and "secretory granule lumen" correlated with PER3 regulation in BRCA and LUAD. Moreover, in molecular functions (MF) analysis, PER3 was correlated with functions related to signal transduction and ion transport, such as "signaling receptor activator activity", "receptor ligand activity", and "passive transmembrane transporter activity" in COAD, HNSC, KIRP, LUAD, and UCEC. "hormone activity" was associated with PER3 function in COAD, KIRP, and LUAD. Universally, "neuroactive ligand-receptor interaction" was extensively enriched in KEGG pathway analysis of COAD, KIRP, LUAD, and UCEC. "IL-17 signaling pathway" was correlated with PER3 in BRCA and UCEC.

PER3 inhibits KIRP and LUAD progression in vitro and in vivo

Considering the consistent tumor suppression function demonstrated in the preceding results, we selected KIRP and LUAD for validation in cell trials. Initially, KIRP cell lines 786-O and Caki-1 exhibited lower PER3 expression compared with normal HK-2 cells ($P<0.05$) (Fig. 8A–B). Upon lentivirus infection, PER3 was overexpressed in 786-O and Caki-1, while silenced in HK-2 ($P<0.05$) (Figs. 8C–E and 9A–B). The results of colony formation and CCK-8 assays demonstrated that PER3 overexpression suppressed, while PER3 silence promoted tumor cell proliferation ($P<0.05$) (Figs. 8F–H and 9C–D). The

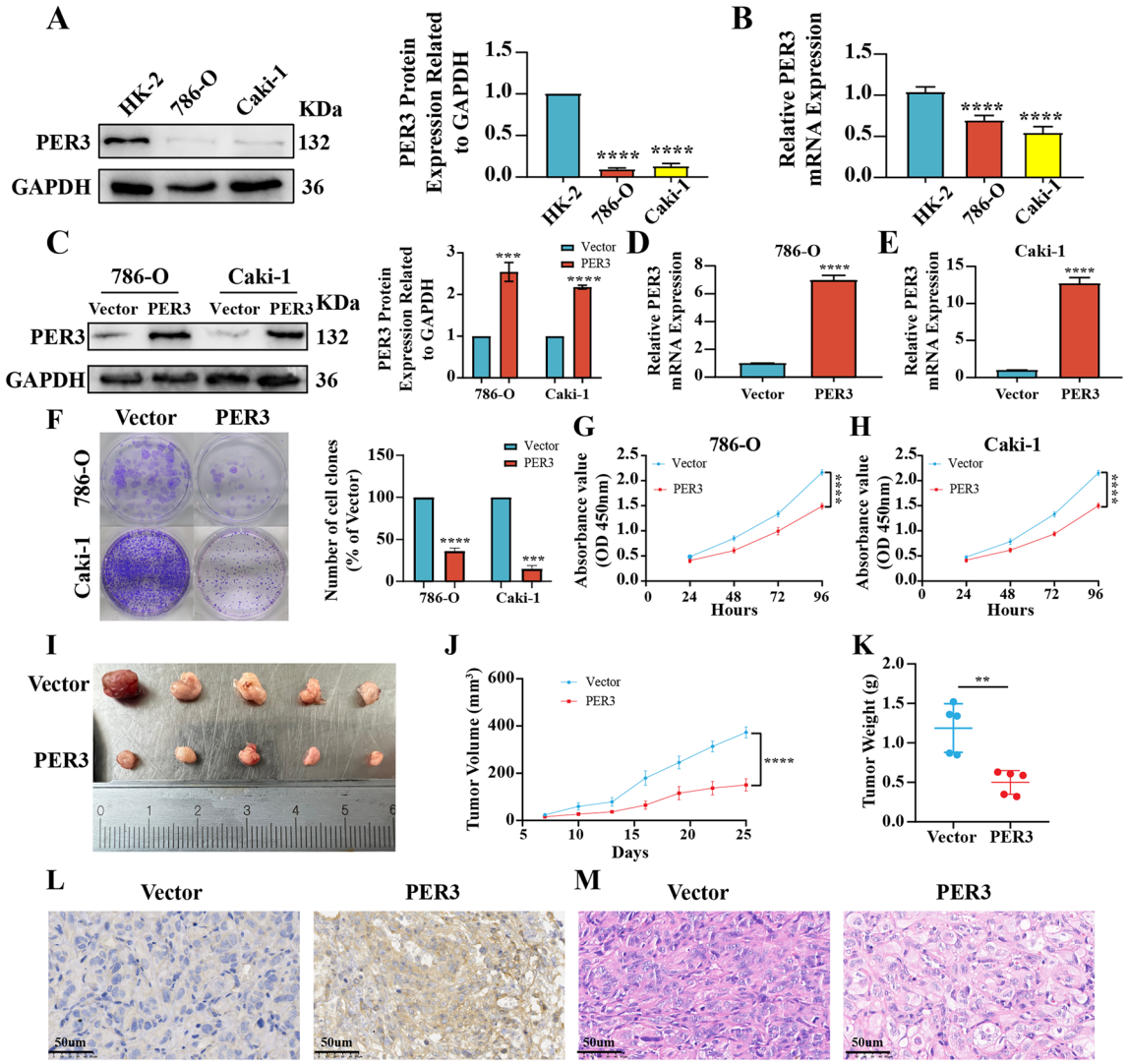

Fig. 8 PER3 inhibited KIRP progression in vitro and in vivo. **A**–**B** PER3 **A** protein and **B** mRNA expression in HK-2 and KIRP [786-O and Caki-1] cells. PER3 **D**–**E** mRNA and **C** protein expression in PER3-overexpressed KIRP cells and their controls. Results of **F** colony formation and **G**–**H** CCK-8 assays of PER3-overexpressed KIRP cells and their controls. **I** Tumor images, **J** tumor volume, **K** tumor weight, **L** PER3 expression, and **M** H&E staining results of the PER3-overexpressed group and the control. All data are representative of three independent experiments. Data are presented as mean ± SD. $^{**}P < 0.01$; $^{***}P < 0.001$; and $^{****}P < 0.0001$

PER3-overexpressed groups demonstrated significantly reduced migration rates (Supplemental Fig. S6A, B) and cell numbers for migration and invasion (Supplemental Fig. S6C, D) compared with the control groups ($P < 0.05$). On the contrary, the knockdown of PER3 enhanced the migration and invasion capacities of HK-2 ($P < 0.05$) (Supplemental Fig. S7A, B). Moreover, we also explored the impact of PER3 overexpression in A549 cells. Cell proliferation, migration, and invasion of A549 were inhibited after PER3 was overexpressed, which coincided with KIRP ($P < 0.05$) (Fig. 9E–H and S7C, D). In vivo experiment results revealed that the tumor weight and volume in the PER3-786-O group were significantly lower than those in the vector-786-O group (Fig. 8I–K) ($P < 0.05$). IHC results revealed that PER3 expression was upregulated in the tumor of the PER3-786-O group ($P < 0.05$), and H&E staining revealed that the tumor cell density was lower in the PER3-786-O group (Fig. 8L–M). Accordingly, PER3 can inhibit KIRP and LUAD progression in vitro and in vivo.

PER3 promoter CGI cg12258811 hypermethylation suppresses PER3 expression in KIRP

BSP was performed to confirm the methylation status of CGI cg12258811 and its correlation with PER3

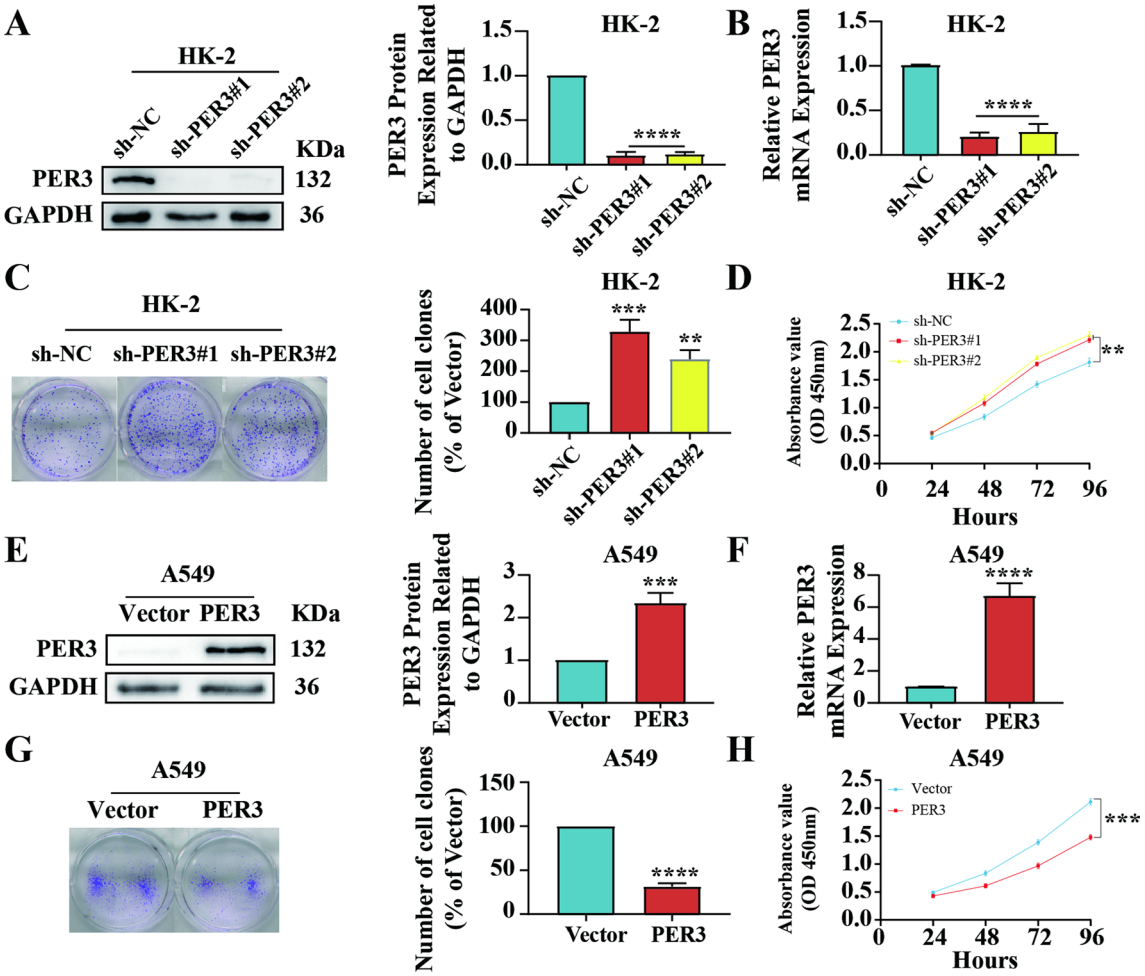

Fig. 9 PER3 silence promoted HK-2 cell proliferation, while PER3 overexpression inhibited A549 proliferation in vitro. **B** and **F** PER3 mRNA and **A** and **C** protein expression in PER3-silenced HK-2 cells, PER3-overexpressed A549 cells, and their controls. Results of **C** and **G** colony formation and **D** and **H** CCK-8 assays of PER3-silenced HK-2 cells, PER3-overexpressed A549 cells, and their controls. All data are representative of three independent experiments. Data are presented as mean ± SD. ***P* < 0.01; ****P* < 0.001; and *****P* < 0.0001

expression in KIRP. The DNA sequence of CGI cg12258811 was examined using the MethPrimer website (https://urogene.org/cgi-bin/methprimer/methprimer.cgi). Cg12258811, comprising three CG sites, was situated 379–392 bp downstream of the PER3 transcriptional start site (circled). The CG at 384 bp, which exhibited the most significant change (underlined), was used for statistical analysis (Fig. 10A). The methylation level of CGI cg12258811 in KIRP cell lines (786-O and Caki-1) was significantly higher than that in the HK-2 cells ($P < 0.0001$) (Fig. 10B–C), indicating CGI cg12258811 hypermethylation in KIRP. DAC treatment significantly reduced CGI cg12258811 methylation levels (Fig. 10B–D) while increasing PER3 mRNA levels in 786-O and Caki-1 cells ($P < 0.001$) (Fig. 10E). These findings suggest that CGI cg12258811 hypermethylation is associated with PER3 downregulation. We further assessed the effect of DAC on the function of KIRP cells. The results indicated that the proliferation, migration, and invasion capacities of 786-O and Caki-1 were suppressed after DAC treatment ($P < 0.05$) (Supplemental Fig. S7E–H). This is consistent with the effect of PER3 overexpression on KIRP.

Discussion

In this study, PER3 mRNA expression was downregulated in 22 cancers, and upregulated in 6 cancers, consistent with previous studies [9, 15, 36]. Survival analyses revealed that higher PER3 expression was associated with improved prognoses in BRCA, CESC, ESCA, CESC, HNSC, KIRP, LUAD, and UCS, whereas high PER3 expression was associated with poor prognoses in ACC, COAD, STAD, and UCEC. However, the results of DSS and PFI analyses contradicted that of the OS analysis in THYM, indicating that the correlation

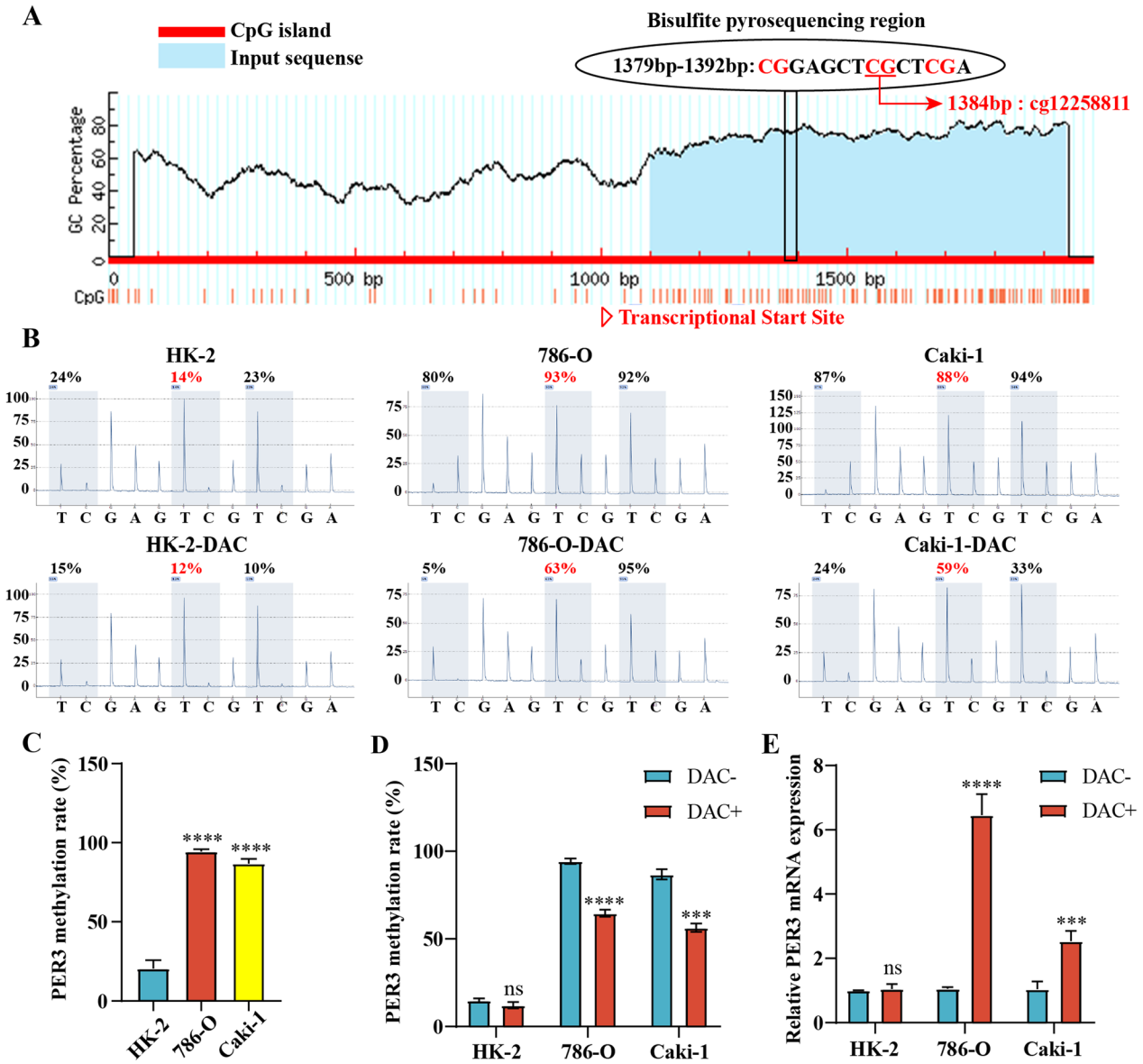

Fig. 10 CGI cg12258811 hypermethylation suppressed PER3 expression in KIRP. **A** Schematic of the BSP region in the PER3 promoter. Input sequence: red region; CGIs: blue region; circled words: CG sites for BSP; underlined magenta words: the most significantly altered CG site in the detected sequence. Representative BSP analysis results of the PER3 promoter CGIs in **B** HK-2, 786-O, and Caki-1 cells before and after DAC treatment. Magenta words: CG site of cg12258811. Average methylation levels **C** in HK-2 and KIRP (786-O and Caki-1) cells and **D** in HK-2 and KIRP cells before and after DAC treatment. **E** PER3 mRNA levels in HK-2 and KIRP cells before and after DAC treatment. All data are representative of three independent experiments. Data are presented as mean ± SD. ns, not significant; ***$P < 0.001$; and ****$P < 0.0001$

between PER3 expression and THYM prognosis requires further investigation. Based on the results of PER3 expression and its association with clinical characteristics and prognosis in pan-cancer, we speculate that PER3 acts as a tumor suppressor in many cancers but causes poor prognosis in others. We further investigated the specific reasons for PER3 expression variation in pan-cancer.

The results of PER3 promoter methylation level analyses in pan-cancer revealed that the promoter methylation level of PER3 was significantly higher in 11 cancers than in normal tissues, confirming that hypermethylation of the PER3 promoter is common in many cancers. However, not all tumors exhibited a correlation between promoter hypermethylation and PER3 transcriptional downregulation. We attempted to explain the

phenomenon of reduced PER3 expression but unchanged promoter methylation levels in some cancers by analyzing PER3 transcription factor expression profiles. After comparison, in all tumor types with reduced PER3 expression, the only tumor type with unchanged promoter methylation and low CLOCK/BMAL1 expression was BLCA, and there was simultaneous promoter hypermethylation and low CLOCK/BMAL1 expression in BRCA, COAD, KIRP, LUAD, PRAD, and UCEC. These results suggest that PER3 expression in cancers was inhibited jointly by promoter hypermethylation and downregulation of transcription factors. In LIHC and STAD with low PER3 expression, CLOCK and BMAL1 were simultaneously upregulated, and the methylation levels did not change. This may involve other epigenetic modifications of non-coding RNA and chromatin remodeling, which needs further study.

To establish the relationship between promoter methylation level, expression level, and PER3 prognosis, six cancers (BRCA, COAD, HNSC, KIRP, LUAD, and UCEC) were selected for in-depth research because all results of promoter methylation level, expression level, and prognosis analysis of PER3 were statistically significant. We discovered that the hypermethylation of promoter CGIs cg12258811 and cg14204433 was associated with decreased PER3 expressions in all six cancers. Furthermore, promoter hypermethylation in BRCA and LUAD resulted in poor OS. The hypermethylation of promoter CGIs cg12258811 in KIRP and cg11843502 in LUAD was associated with reduced OS. However, high methylation levels of CGI cg14204433 improved OS in UCEC. The expression-related prognostic analysis revealed that high PER3 expression can improve outcomes in patients with BRCA, HNSC, LUAD, and KIRP but can hinder prognosis in COAD and UCEC. As expected, the effect of promoter (or specific promoter CGIs) methylation level on OS in BRCA, LUAD, KIRP, and UCEC contradicted that of PER3 expression.

Furthermore, the methylation level of the PER3 promoter and PER3 expression were correlated with cancer stages. In KIRP, promoter hypermethylation and low PER3 expression resulted in advanced individual cancer stages. Conversely, in UCEC, hypomethylation of the PER3 promoter and high expression were associated with cancer stage development. The negative regulation of PER3 expression by the CGI 12558811 methylation level in KIRP was validated by BSP and RT-qPCR tests. The inhibitory role of PER3 on KIRP and LUAD progression was validated in vitro and in vivo. Notably, DAC reduced PER3 promoter (cg12258811) methylation levels, increased its expression, and inhibited KIRP cell functions, which provides a new theoretical basis for treating tumors with epigenetic drugs.

As a component of the tumor microenvironment, immune cells play a critical role in the carcinogenesis of many cancers [37, 38]. In most of the six cancers studied, PER3 upregulation was associated with higher infiltrations of TCM cells, T helper cells, eosinophils, mast cells, and NK cells. The anti-tumor effect of these immune cells has been demonstrated in many previous studies [39–43]. In BRCA and KIRP, PER3 levels were negatively correlated with Treg cell infiltration. These findings provide immunological evidence for the anti-tumor role of PER3. Immune-related BP and the "IL-17 signaling pathway" were associated with PER3 expression in BRCA and UCEC, which provided further evidence that immune function is involved. Moreover, hormone-related BP, neurological function-related CC, and signal transduction and ion transport-related MF were identified as common PER3-triggered molecular mechanisms. Noticeably, "neuroactive ligand-receptor interaction" was extensively enriched in the KEGG pathway analysis, providing a valuable direction for the study of downstream signaling pathways.

Overall, we observed strong associations between PER3 promoter hypermethylation, especially in CGIs cg12258811 and cg14204433, and reduced expression across the six cancers. Increased PER3 expression improved prognosis in BRCA, HNSC, KIRP, and LUAD but worsened outcomes in COAD and UCEC. Furthermore, a direct relationship between promoter methylation status and prognosis was discovered in BRCA, KIRP, LUAD, and UCEC. Specifically, promoter hypermethylation and PER3 downregulation in KIRP, but promoter hypomethylation and PER3 upregulation in UCEC were associated with advanced individual cancer stages. These findings suggest that promoter hypermethylation in BRCA, HNSC, KIRP, and LUAD may promote cancer progression by downregulating PER3 expression.

Conclusions

In conclusion, our findings identified PER3 as a prognostic marker in pan-cancer and elucidated the epigenetic mechanism underlying PER3 expression variation. Our findings provide a valuable foundation for further research on PER3 and its promoter methylation in cancer, which may contribute to tumor treatment and prognosis.

Abbreviations

PER3	Period circadian regulator 3
CGIs	CpG islands
KIRP	Kidney renal papillary cell carcinoma
LUAD	Lung adenocarcinoma
HNSC	Head and neck squamous cell carcinoma
KIRC	Kidney renal clear cell carcinoma
TCGA	The cancer genome atlas
OS	Overall survival
DSS	Disease-specific survival
PFI	Progression-free interval

K–M	Kaplan–Meier
EWAS	Epigenome-wide association study
BRCA	Breast invasive carcinoma
COAD	Colon adenocarcinoma
UCEC	Uterine corpus endometrial carcinoma
DEGs	Differentially expressed genes
KEGG	Kyoto encyclopedia of genes and genomes
GO	Gene ontology
FBS	Fetal bovine serum
DAC	Decitabine
BSP	Bisulfite pyrosequencing
SD	Standard deviation
LGG	Brain lower grade glioma
THYM	Thyroid carcinoma, and thymoma
HR	Hazard ratio
CESC	Cervical squamous cell carcinoma and endocervical adenocarcinoma
ESCA	Esophageal carcinoma
UCS	Uterine carcinosarcoma
ACC	Adrenocortical carcinoma
STAD	Stomach adenocarcinoma
BLCA	Bladder urothelial carcinoma
TCM	Central memory T
NK	Natural killer (NK)
Treg	Regulatory T
BP	Biological processes
CC	Cellular components
MF	Molecular functions

Supplementary Information

The online version contains supplementary material available at https://doi.org/10.1186/s13148-024-01760-5.

Additional file 1.

Acknowledgements
We thank Home for Researchers editorial team (www.home-for-researchers.com) for language editing service.

Authors' contributions
M. Y. conceived and guided the research and revised the manuscript. Y. L. conducted the experiments, collected the data, and drafted the manuscript. W. L. analyzed the data and contributed to the animal models. J. D. assisted in data analyses. All authors reviewed the manuscript.

Funding
This work was jointly sponsored by Natural Science Foundation of Chongqing, China (CSTB2024NSCQ-MSX0761); the Chongqing Wanzhou Municipal Science and Health Joint Research Project (Grant No. wzstc-kw2023039); the Chongqing Natural Science Foundation (Grant No. CSTB2023NSCQ-BHX0047); the Chongqing Science and Health Joint Scientific Research Project on Traditional Chinese Medicine (Grant No. 2024ZYQN001); Chongqing Wanzhou social science key topics (Grant No. WZKT2024086); the Natural Science Foundation of China (Grant No. 82073020).

Availability of data and materials
The data supporting this study was obtained from TCGA (https://portal.gdc.cancer.gov/projects/), UALCAN (https://ualcan.path.uab.edu/), MEXPRESS (https://mexpress.be/), EWAS Data Hub (https://ngdc.cncb.ac.cn/ewas/datahub/), and MethSurv (https://biit.cs.ut.ee/methsurv/) public databases.

Declarations

Ethics approval and consent to participate
All animal experiments were approved by Institutional Animal Care and Use of Chongqing Medical University (approval number: IACUC-CQMU-2024-0462).

Consent for publication
Not applicable.

Competing interests
The authors declare no competing interests.

Received: 26 July 2024 Accepted: 7 October 2024
Published online: 14 October 2024

References

1. 2024 Global cancer burden growing amidst mounting need for services Saudi Med J 45(3): 326–327
2. Siegel RL, Miller KD, Jemal A. Cancer statistics, 2019. CA Cancer J Clin. 2019;69(1):7–34.
3. Liu B, Fan Y, Song Z, Han B, Meng Y, Cao P, et al. Identification of DRP1 as a prognostic factor correlated with immune infiltration in breast cancer. Int Immunopharmacol. 2020;89(Pt B): 107078.
4. Shafi AA, Knudsen KE. Cancer and the circadian clock. Cancer Res. 2019;79(15):3806–14.
5. Mohawk JA, Green CB, Takahashi JS. Central and peripheral circadian clocks in mammals. Annu Rev Neurosci. 2012;35:445–62.
6. Takahashi JS, Hong HK, Ko CH, McDearmon EL. The genetics of mammalian circadian order and disorder: implications for physiology and disease. Nat Rev Genet. 2008;9(10):764–75.
7. Orhan T, Nielsen PB, Hviid TVF, Rosen AW, Gogenur I. Expression of circadian clock genes in human colorectal cancer tissues using droplet digital PCR. Cancer Invest. 2019;37(2):90–8.
8. Wang X, Yan D, Teng M, Fan J, Zhou C, Li D, et al. Reduced expression of PER3 is associated with incidence and development of colon cancer. Ann Surg Oncol. 2012;19(9):3081–8.
9. Liu Y, Wu Z, Li Y, Zhang J, Gao Y, Yuan G, et al. PER3 plays anticancer roles in the oncogenesis and progression of breast cancer via regulating MEK/ERK signaling pathway. J Chin Med Assoc. 2022;85(11):1051–60.
10. Lesicka M, Jablonska E, Wieczorek E, Seroczynska B, Siekierzycka A, Skokowski J, et al. Altered circadian genes expression in breast cancer tissue according to the clinical characteristics. PLoS ONE. 2018;13(6): e0199622.
11. Jin Y, Wang Z, Huang S, Liu C, Wu X, Wang H. Identify and validate circadian regulators as potential prognostic markers and immune infiltrates in head and neck squamous cell carcinoma. Sci Rep. 2023;13(1):19939.
12. Zhou L, Luo Z, Li Z, Huang Q. Circadian clock is associated with tumor microenvironment in kidney renal clear cell carcinoma. Aging. 2020;12(14):14620–32.
13. Li Q, Xia D, Wang Z, Liu B, Zhang J, Peng P, et al. Circadian rhythm gene PER3 negatively regulates stemness of prostate cancer stem cells via WNT/beta-catenin signaling in tumor microenvironment. Front Cell Dev Biol. 2021;9: 656981.
14. Zhang F, Sun H, Zhang S, Yang X, Zhang G, Su T. Overexpression of PER3 inhibits self-renewal capability and chemoresistance of colorectal cancer stem-like cells via inhibition of notch and beta-catenin signaling. Oncol Res. 2017;25(5):709–19.
15. Cai DW, Chen D, Sun SP, Liu ZJ, Liu F, Xian SZ, et al. Overexpression of PER3 reverses paclitaxel resistance of prostate cancer cells by inhibiting the Notch pathway. Eur Rev Med Pharmacol Sci. 2018;22(9):2572–9.
16. Li YY, Jin F, Zhou JJ, Yu F, Duan XF, He XY, et al. Downregulation of the circadian period family genes is positively correlated with poor head and neck squamous cell carcinoma prognosis. Chronobiol Int. 2019;36(12):1723–32.
17. Sahar NE, Qadir J, Riaz SK, Bagabir SA, Muneer Z, Sheikh AK, et al. Dysregulated expression of suppressor loop of circadian rhythm genes in colorectal cancer pathogenesis. Minerva Med. 2022;113(3):497–505.
18. Zhang J, Jiang H, Du K, Xie T, Wang B, Chen C, et al. Pan-cancer analyses reveal genomics and clinical characteristics of the melatonergic regulators in cancer. J Pineal Res. 2021;71(3): e12758.
19. Climent J, Perez-Losada J, Quigley DA, Kim IJ, Delrosario R, Jen KY, et al. Deletion of the PER3 gene on chromosome 1p36 in recurrent ER-positive breast cancer. J Clin Oncol. 2010;28(23):3770–8.

20. Zhu Y, Stevens RG, Hoffman AE, Fitzgerald LM, Kwon EM, Ostrander EA, et al. Testing the circadian gene hypothesis in prostate cancer: a population-based case-control study. Cancer Res. 2009;69(24):9315–22.
21. You JS, Jones PA. Cancer genetics and epigenetics: two sides of the same coin? Cancer Cell. 2012;22(1):9–20.
22. Baylin SB, Jones PA. A decade of exploring the cancer epigenome—biological and translational implications. Nat Rev Cancer. 2011;11(10):726–34.
23. Dawson MA, Kouzarides T. Cancer epigenetics: from mechanism to therapy. Cell. 2012;150(1):12–27.
24. Agrawal K, Das V, Vyas P, Hajduch M. Nucleosidic DNA demethylating epigenetic drugs—a comprehensive review from discovery to clinic. Pharmacol Ther. 2018;188:45–79.
25. Hansen KD, Timp W, Bravo HC, Sabunciyan S, Langmead B, McDonald OG, et al. Increased methylation variation in epigenetic domains across cancer types. Nat Genet. 2011;43(8):768–75.
26. Tang W, Peng W, Zhang H, Zhang Y, Li B, Duan C. Period 3, a tumor suppressor in non-small cell lung cancer, is silenced by hypermethylation. Int J Clin Exp Pathol. 2018;11(1):120–8.
27. Yao M, Fu L, Liu X, Zheng D. In-silico multi-omics analysis of the functional significance of calmodulin 1 in multiple cancers. Front Genet. 2021;12:793508.
28. Chandrashekar DS, Bashel B, Balasubramanya SAH, Creighton CJ, Ponce-Rodriguez I, Chakravarthi B, et al. UALCAN: a portal for facilitating tumor subgroup gene expression and survival analyses. Neoplasia. 2017;19(8):649–58.
29. Koch A, Jeschke J, Van Criekinge W, van Engeland M, De Meyer T. MEXPRESS update 2019. Nucleic Acids Res. 2019;47(W1):W561–5.
30. Xiong Z, Li M, Yang F, Ma Y, Sang J, Li R, et al. EWAS Data Hub: a resource of DNA methylation array data and metadata. Nucleic Acids Res. 2020;48(D1):D890–5.
31. Modhukur V, Iljasenko T, Metsalu T, Lokk K, Laisk-Podar T, Vilo J. MethSurv: a web tool to perform multivariable survival analysis using DNA methylation data. Epigenomics. 2018;10(3):277–88.
32. Hanzelmann S, Castelo R, Guinney J. GSVA: gene set variation analysis for microarray and RNA-seq data. BMC Bioinformatics. 2013;14:7.
33. Bindea G, Mlecnik B, Tosolini M, Kirilovsky A, Waldner M, Obenauf AC, et al. Spatiotemporal dynamics of intratumoral immune cells reveal the immune landscape in human cancer. Immunity. 2013;39(4):782–95.
34. He M, Zuo C, Wang J, Liu J, Jiao B, Zheng J, et al. Prognostic significance of the aggregative perivascular growth pattern of tumor cells in primary central nervous system diffuse large B-cell lymphoma. Neuro Oncol. 2013;15(6):727–34.
35. Li LC, Dahiya R. MethPrimer: designing primers for methylation PCRs. Bioinformatics. 2002;18(11):1427–31.
36. Wu Y, Tao B, Zhang T, Fan Y, Mao R. Pan-cancer analysis reveals disrupted circadian clock associates with T cell exhaustion. Front Immunol. 2019;10:2451.
37. Hanahan D, Coussens LM. Accessories to the crime: functions of cells recruited to the tumor microenvironment. Cancer Cell. 2012;21(3):309–22.
38. Bagaev A, Kotlov N, Nomie K, Svekolkin V, Gafurov A, Isaeva O, et al. Conserved pan-cancer microenvironment subtypes predict response to immunotherapy. Cancer Cell. 2021;39(6):845-865e.7.
39. Klebanoff CA, Gattinoni L, Restifo NP. Sorting through subsets: which T-cell populations mediate highly effective adoptive immunotherapy? J Immunother. 2012;35(9):651–60.
40. Basu A, Ramamoorthi G, Albert G, Gallen C, Beyer A, Snyder C, et al. Differentiation and regulation of T(H) cells: a balancing act for cancer immunotherapy. Front Immunol. 2021;12: 669474.
41. Grisaru-Tal S, Rothenberg ME, Munitz A. Eosinophil-lymphocyte interactions in the tumor microenvironment and cancer immunotherapy. Nat Immunol. 2022;23(9):1309–16.
42. Lichterman JN, Reddy SM. Mast cells: a new frontier for cancer immunotherapy. Cells. 2021;10(6):1270.
43. Shimasaki N, Jain A, Campana D. NK cells for cancer immunotherapy. Nat Rev Drug Discov. 2020;19(3):200–18.

Publisher's Note